SCIENTIFIC REPORTS

OPEN

SUBJECT AREAS:
SINGLE-MOLECULE BIOPHYSICS
BIOENERGETICS

Received
28 February 2014

Accepted
24 April 2014

Published
14 May 2014

Correspondence and requests for materials should be addressed to H.N. (hnoji@appchem.t.u-tokyo.ac.jp)

Characterization of the temperature-sensitive reaction of F_1-ATPase by using single-molecule manipulation

Rikiya Watanabe[1,2] & Hiroyuki Noji[1]

[1]Department of Applied Chemistry, School of Engineering, The University of Tokyo, Bunkyo-ku, Tokyo 113-8656, Japan, [2]PRESTO, JST, Bunkyo-ku, Tokyo 113-8656, Japan.

F_1-ATPase (F_1) is a rotary motor protein that couples ATP hydrolysis to mechanical rotation with high efficiency. In our recent study, we observed a highly temperature-sensitive (TS) step in the reaction catalyzed by a thermophilic F_1 that was characterized by a rate constant remarkably sensitive to temperature and had a Q_{10} factor of 6–19. Since reactions with high Q_{10} values are considered to involve large conformational changes, we speculated that the TS reaction plays a key role in the rotation of F_1. To clarify the role of the TS reaction, in this study, we conducted a stall and release experiment using magnetic tweezers, and assessed the torque generated during the TS reaction. The results indicate that the TS reaction generates the same amount of rotational torque as does ATP binding, but more than that generated during ATP hydrolysis. Thus, we confirmed that the TS reaction contributes significantly to the rotation of F_1.

F_1-ATPase ($\alpha_3\beta_3\gamma\delta\varepsilon$), a catalytic subcomplex of F_oF_1-ATP synthase, is a rotary motor protein fuelled by ATP hydrolysis[1–4]. The $\alpha_3\beta_3\gamma$ subcomplex functions as the minimum component of the rotating system, in which the $\alpha_3\beta_3$ subunits form a cylindrical stator and the γ rotor subunit penetrates the center of the cylinder[5–7]. The catalytic sites for ATP hydrolysis/synthesis are located at the interface between each α and β subunit, mainly on the β subunits; i.e., F_1 possesses three catalytic sites. The rotary motion of F_1 can be visualized under an optical microscope[8–10]. Upon ATP hydrolysis, F_1 rotates in the anticlockwise direction (when viewed from the membrane side), in which the three β subunits cooperatively change their conformation, generating a rotational torque of 40 pN·nm rad^{-1} for the F_1 from thermophilic *Bacillus* PS3[11] and 20–74 pN·nm rad^{-1} for the F_1 from *Escherichia coli*[10,12,13]. The energy required for the mechanical work for one γ rotation is balanced by the hydrolysis of three ATP molecules. Therefore, F_1 is extremely efficient in converting chemical energy to mechanical work and the catalysis is tightly coupled to the mechanical work[11,14].

The mechanisms underlying the catalysis and the rotation have been established[15], although some uncertainties still exist[3,16,17]. According to the presently accepted scheme of the reaction (Fig. 1), hydrolysis or turnover of a single ATP molecule at each catalytic site is coupled with one revolution of the γ subunit, and the angle between the three catalytic sites differs by 120° during each catalytic phase[18]. The step size of the rotation is 120°, each coupled to the turnover of a single ATP molecule[11]. The 120° step is further divided into 80° and 40° substeps[19,20]. The 80° substep is triggered by ATP binding and ADP release[21–23], whereas the 40° substep is triggered by ATP hydrolysis and the release of inorganic phosphate (P_i)[15,18,20,22]. The angular positions of F_1 before the 80° and 40° substeps are referred to as the ATP-binding and catalytic angles, respectively. When a β subunit's ATP-binding angle is 0° (cyan circle in Fig. 1), it executes a hydrolysis reaction after the γ subunit rotates by 200°[18], releases ADP between 240° and 320°, and P_i at 320°, respectively[15,24].

Using rotation assays, we recently detected the presence of a new reaction intermediate as a clear intervening pause before the 80° substep during the rotation of F_1, by using F_1 from the thermophilic *Bacillus* PS3 (TF_1) at low temperatures (~9°C)[25,26]. The thermophilic *Bacillus* PS3 grows at 65°C, a temperature higher than that at which other species can grow. The new reaction intermediate was also observed in the rotation assay at room temperature (~28°C) using a mutant TF_1 in which a glutamate residue at position 190 of the β-subunit (corresponding to Glu-181 of the F_1 from *Escherichia coli* and Glu-188 of the F_1 from bovine mitochondria) was substituted

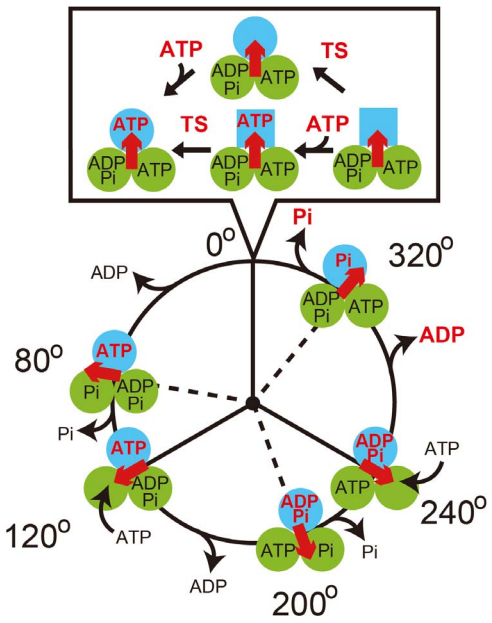

Figure 1 | Reaction scheme of F_1 The circles and red arrows represent the catalytic states of the β subunits and the angular positions of the γ subunit, respectively. Each β subunit hydrolyzes a single molecule of ATP during one turn of γ, whereas three β subunits differ the reaction phase by 120°. The catalytic state of the top β subunit (cyan) has been indicated for clarity. ATP binding, TS reaction, hydrolysis, ADP release, and P_i release occur at 0°, 0°, 200°, 240°, and 320°, respectively.

with an aspartic acid[26,27]. Glu-190 of the β-subunit of TF_1 has been identified as a critical residue in ATP hydrolysis[5,28–30], and is termed the "general base" since this residue seems to induce an in-line attack of the water molecule on the γ phosphate and initiate the hydrolysis reaction by activating the water molecule. Another single molecule study revealed that this new reaction intermediate occurs at the angle where the β subunit waits for ATP binding (0° in Fig. 1)[26]. Although this reaction has not been further characterized, the rate constant was found to be remarkably sensitive to temperature. The rate constant increased by a factor of 6–19 for every 10°C rise in temperature[25,26] (Q_{10} = 6–19), which was unusually high compared to conventional Q_{10} values of around 2. In general, reactions with high Q_{10} values involve large conformational changes. Therefore, this reaction may play a key role in rotation and torque generation. Hereafter, this reaction has been referred to as the temperature-sensitive reaction (TS reaction).

To evaluate the torque generated during each step of the reaction, we recently developed a novel method to measure the equilibrium constant of the F_1 reaction at various rotational angles[31]. Through this method, we arrested F_1 in the transient conformation using magnetic tweezers and observed the behavior of F_1 immediately after release from arrest. From the analysis of the behavior of F_1, we could simultaneously determine the rate constant for each forward and reverse step of the reaction at various rotational angles. Thus, we could measure the equilibrium constant of each step of the reaction. Because the equilibrium constant is a measure of the difference in the free energy of the pre- and post-reaction states, $\Delta G(\theta) = -k_B T \cdot \ln K_E(\theta)$, the torque generated during the reaction can be estimated from the derivative of the free energy, $d\Delta G(\theta)/d\theta$.

In the present study, we perform a stalling experiment to elucidate how F_1 modulates the rate and equilibrium constants of the TS reaction as a function of the rotational angle and attempt to assess its contribution in torque generation. The results will contribute to understanding the chemomechanical energy coupling of F_1 at the resolution of the elementary reaction step.

Results

Temperature dependence of the rotation of the TF_1(βE190D) mutant. We observed the rotation of the mutant TF_1, namely, $\alpha_3\beta(E190D)_3\gamma$, in the presence of 1 mM ATP at 18, 23, and 28°C (Fig. 2a). Between 18 and 28°C, the mutant F_1 rotated with 80° and 40° substeps (Fig. 2b); the rate limiting steps of the 80° and 40° substeps were identified to be the TS reaction and ATP hydrolysis, respectively, in our previous study[26]. The dwell time prior to the 80° substep (TS dwell) showed a strong dependence on temperature (Fig. 2c). By fitting the histograms with exponential functions, the time constants of the TS reaction at 18, 23, and 28°C were determined to be 330, 96, and 43 ms, respectively (Fig. 2c). In contrast, the dwell time before the 40° substep (hydrolysis dwell) was not dependent on temperature and was determined to be 208 ms for 18°C, 235 ms for 23°C, and 270 ms for 28°C (Fig. 2d). These results were consistent with the results of our previous study on the TS reaction[26].

Manipulation of single F_1 rotation. For manipulating the rotation of the γ subunit of F_1, a magnetic bead (ϕ ≈ 200 nm) was attached to it and the $\alpha_3\beta_3$ ring was immobilized on the glass surface. For the stalling experiments, the rotation of F_1 was observed under conditions under which the TS dwell was lengthened enough to

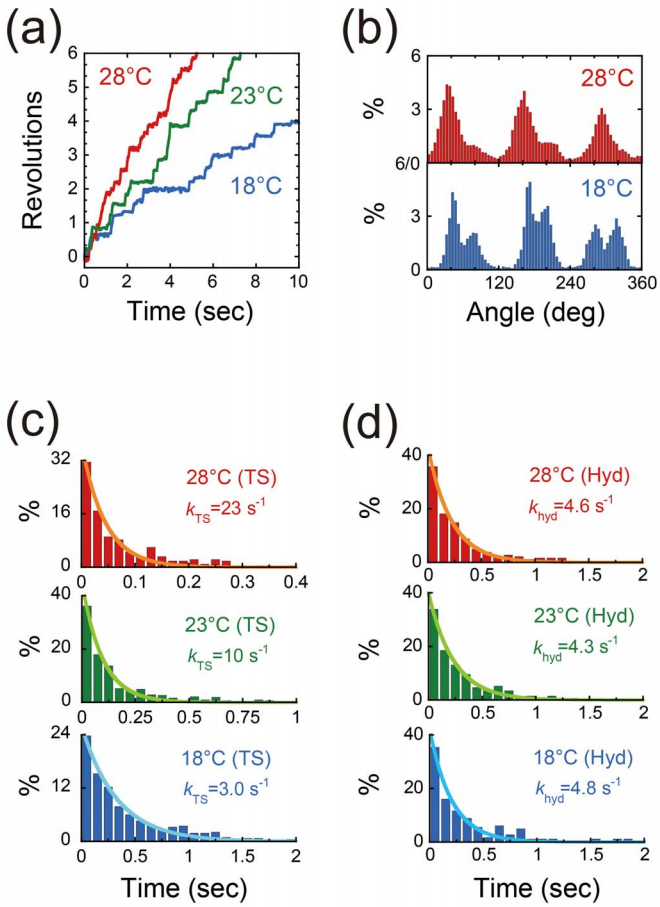

Figure 2 | Rotation of mutant F_1 ($\alpha_3\beta(E190D)_3\gamma$) at various temperatures. (a). Time course of rotation of the mutant F_1 in the presence of 1 mM ATP at 18 (blue), 23 (green), and 28°C (red). (b). Histograms of the angular position during rotation as calculated from Fig. 2a. (c, d). Histograms of the dwell time of the pause prior to the 80° substep (TS dwell) or the 40° substep (hydrolysis dwell). Curves were plotted using a single-order reaction scheme. $y = C \cdot \exp(-kt)$, where $k_{TS}^{on}(18°C)$ = 3.0 s^{-1}, $k_{TS}^{on}(23°C)$ = 10 s^{-1}, $k_{TS}^{on}(28°C)$ = 23 s^{-1}, $k_{hyd}(18°C)$ = 4.8 s^{-1}, $k_{hyd}(23°C)$ = 4.3 s^{-1}, and $k_{hyd}(28°C)$ = 4.6 s^{-1}.

enable recording at approximately 1,000 fps using a mutant F_1, $\alpha_3\beta(E190D)_3\gamma$. As mentioned above, we can distinguish between the angular positions for the TS reaction and the hydrolysis by analyzing the TS and hydrolysis dwell times (Figs. 2c, 2d). When F_1 paused for the TS reaction, we turned on the magnetic tweezers to arrest F_1 at the target angle (Fig. 3a). After the set period had elapsed, we turned off the magnetic tweezers and released F_1 from the arrest. Following release, F_1 showed one of two behaviors: rotating directly forward to the next catalytic angle (red in Fig. 3b), i.e., skipping the pause at the original ATP-binding angle, or returning to the original ATP-binding angle (blue in Fig. 3b) without exception. Forward rotation of F_1 implied that it had completed the TS reaction and exerted a torque on the magnetic beads; backward rotation of F_1 meant that it had not completed the TS reaction because it did not catalyze the reaction and hence could not generate a torque. These behaviors of F_1 are hereafter referred to as "ON" (forward rotation) and "OFF" (backward rotation), respectively. Using the above-mentioned methodology, we conducted the stalling experiments in the angle range of $\pm 50^\circ$, where the standard deviation of the arrested angle was 5.8°. The following sections discuss the analysis of the probability (P_{ON}) of ON events against the total trials.

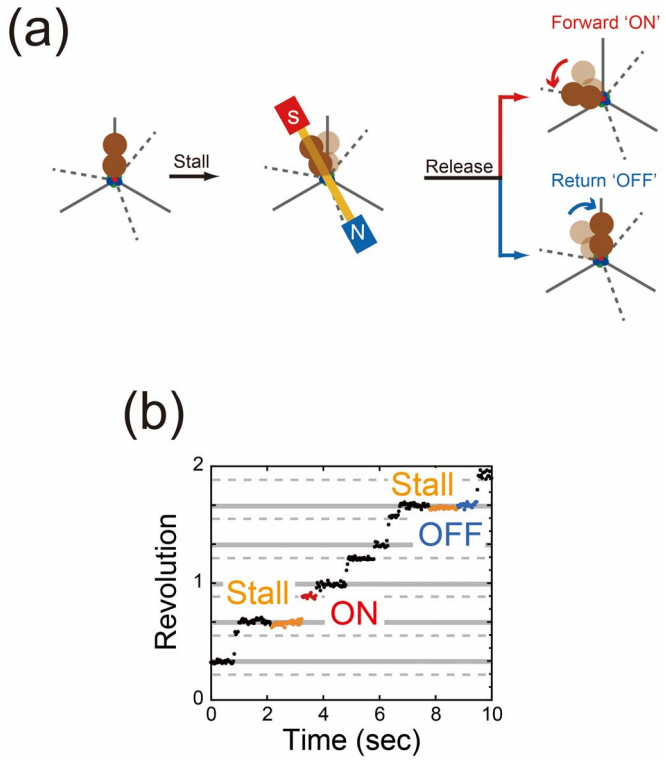

Figure 3 | Single-molecule manipulation of F_1. (a). Schematic image of the manipulation procedures. The gray solid and dashed lines represent the ATP-binding and catalytic angles, respectively. When F_1 paused due to TS dwell at the ATP-binding angle, the magnetic tweezers were switched on to stall F_1 at the target angle and then turned off to release the motor after the set period had elapsed. A released F_1 showed forward (ON) or backward (OFF) rotation with respect to the original ATP binding angle. The behavior of F_1 indicated whether the TS reaction was completed (in case of ON) or not (in case of OFF). (b). Examples of stalling experiments for the TS reaction at 18°C. During a pause, F_1 was stalled at -6.6° from the original pausing angle for 1.0 s and then released. After being released, F_1 rotated to the next catalytic angle without any backward rotation, indicating that the TS reaction had been completed by F_1 upon release (red). When F_1 was stalled at -9.1° for 1.0 s, it rotated back to its original pausing angle, implying that the TS reaction had not been completed (blue).

Angular dependence of the kinetic parameters of the TS reaction. Using the mutant F_1, experiments were conducted at 18°C, where the TS dwell time was 330 ms (Fig. 2c). Fig. 4a shows P_{ON} plotted against the stall time. P_{ON} increased with both the stall angle and the stall time (Fig. 4a), which is similar to our previous observation of ATP binding to wild-type F_1[31]. In addition, P_{ON} did not always saturate to 100% but converged to a certain value, e.g., 60% for $+10^\circ$ stall (green line in Fig. 4a). These observations imply that the TS reaction is reversible, and that reverse reaction also occurs during stalling. Therefore, the plateau level indicates the equilibrium level between the pre- and post-TS reaction states. To confirm the reversibility, we analyzed the behaviors immediately after the OFF events; i.e., dwell times to spontaneously conduct 80° steps (dwell times at 0° in Fig. 1) immediately after the OFF events (blue points in Fig. 3b). Here, to avoid including data from before the equilibrium, only experiments with longer stalling times, in which P_{ON} achieved a plateau were analyzed. The dwell time histogram obtained from all the stall angles showed a single exponential decay, providing a rate constant of 1.1 s^{-1} (bottom panel in Fig. 4b), which corresponded to that obtained for freely rotating F_1s, which were not manipulated with magnetic tweezers (Fig. 2c). This correspondence excluded the possibility of any unexpected inactivation occurring during the stalling that might compete with the TS reaction. We also plotted a histogram of the dwell times to conduct 40° steps (dwell times at 80° in Fig. 1) after the ON events (red points in Fig. 3b). This histogram (top panel in Fig. 4b) was also in good agreement with that obtained for freely rotating F_1s (Fig. 2d), confirming that the manipulation did not alter the kinetic properties of F_1.

By fitting the time courses of P_{ON} based on a reversible reaction scheme, $F_1 \rightleftarrows F_1^*$, the rate constants of the TS reaction and its reverse reaction, $k_{TS}^{on}(18^\circ C)$ and $k_{TS}^{off}(18^\circ C)$, were determined for each stall angle (Figs. 5a and 5b). $k_{TS}^{on}(18^\circ C)$ increased exponentially with the stall angle by approximately 6.2 fold per 20°, which was double that reported previously for ATP binding[31]. $k_{TS}^{on}(18^\circ C)$ at $\pm 0^\circ$ was evidently slower than that determined for freely rotating F_1s. This phenomenon, which is similar to the ATP-binding step, is attributed to thermal agitated rotary fluctuation that occasionally pushes γ forward, accelerating the TS reaction. In contrast, $k_{TS}^{off}(18^\circ C)$ was almost constant at approximately 0.3 s^{-1}. Therefore, the equilibrium constant of the TS reaction [$k_{TS}^{on}(18^\circ C)/k_{TS}^{off}(18^\circ C) = K_E^{TS}(18^\circ C)$] increased 2.2 times from -10° to $+10^\circ$ (blue points in Fig. 5c), which is a steeper angle dependence than that observed for ATP hydrolysis in the previous study[31].

To confirm the strong angle dependence of the TS reaction under a different condition, the stalling experiments were also conducted at 23 and 28°C, where the time constants of the TS reaction were 96 and 43 ms, respectively (Fig. 2c). The time courses of P_{ON} showed the same tendency as that observed at 18°C (Figs. 4c, 4e). The reversibility of the TS reaction at 23 and 28°C was also confirmed from the analysis of the dwell time after arrest (Figs. 4d and 4f). The rate and equilibrium constants were determined as mentioned above (Figs. 5a, 5b, and 5c). The equilibrium constants determined for the TS reaction at 23 and 28°C showed essentially the same angle dependence as that at 18°C (red and green points in Fig. 5c). Thus, the strong angle dependence of the TS reaction is inherent in F_1, regardless of the temperature.

Rotational energy potential. We examined the rotational energy potential during TS dwell, i.e., the waiting state for the TS reaction. The probability distribution of γ-orientation during the TS dwell of mutant F_1, $\alpha_3\beta(E190D)_3\gamma$, was measured (orange points in Fig. 6a). The probability distributions obtained were then transformed into the rotational energy potential according to the Boltzmann's Law, $\Delta G = -k_BT \cdot \ln(P/P_o)$ (orange points in Fig. 6b). The potential determined was fitted to the harmonic function, $\Delta G = 1/2 \cdot \kappa \cdot \theta^2$, where κ is the torsion stiffness. The determined value of stiffness

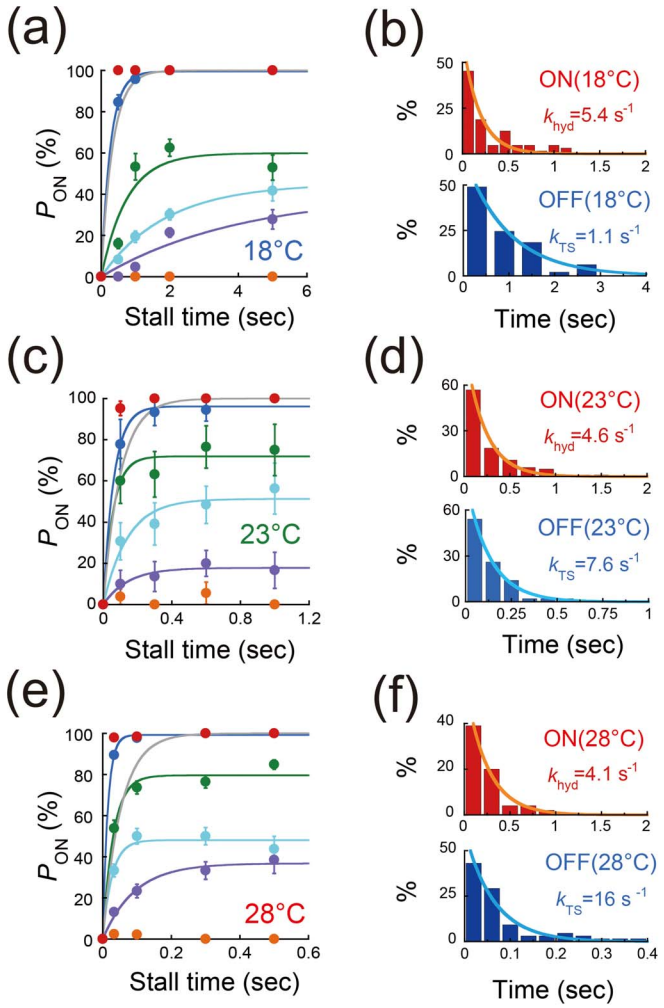

Figure 4 | Angular dependence of the TS reaction by the mutant F_1 ($\alpha_3\beta$(E190D)$_3\gamma$). (a, c, e). Time course of P_{ON} of F_1 ($\alpha_3\beta$(E190D)$_3\gamma$) in the presence of 1 mM ATP at 18, 23, and 28°C, after stalling at −30° (orange), −10° (purple), 0° (cyan), +10° (green), +30° (blue), and +50° (red). The gray lines represent the time courses for freely rotating F_1s. k_{TS}^{on} and k_{TS}^{off} were determined by fitting a single exponential function: $P_{ON} = (k_{TS}^{on}/(k_{TS}^{on} + k_{TS}^{off}))\cdot[1 - \exp(-(k_{TS}^{on} + k_{TS}^{off})\cdot t)]$, according to the reversible reaction scheme, $F_1 \rightleftarrows F_1^*$. Each data point was obtained from 13–63 trials using 4 molecules. The error in P_{ON} is represented as $\sqrt{P_{ON}(100-P_{ON})/N}$, where N is the number of trials for each stall measurement. (b, d, f). Histograms of dwell times immediately after the stalling at 18, 23, and 28°C. Top panels represent the dwell time to conduct another 40° step (hydrolysis dwell) after the ON event (red points in Fig. 3b). Bottom panels represent the dwell time to conduct spontaneously an 80° step after an OFF event (blue points in Fig. 3b). Curves were obtained by fitting the data to a single-order reaction scheme. $y = C\cdot\exp(-kt)$, where $k_{hyd}(18°C) = 5.4\ s^{-1}$, $k_{TS}^{on}(18°C) = 1.1\ s^{-1}$, $k_{hyd}(23°C) = 4.6\ s^{-1}$, $k_{TS}^{on}(23°C) = 7.6\ s^{-1}$, $k_{hyd}(28°C) = 4.1\ s^{-1}$, and $k_{TS}^{on}(28°C) = 16\ s^{-1}$.

was 75 pN·nm, which was similar to the values for ATP binding of wild-type F_1 and hydrolysis of mutant F_1, $\alpha_3\beta$(E190D)$_3\gamma$, determined in the previous study[31] (red and blue points in Fig. 6b). This result suggested that the magnitude of rotational energy potential in the pre-reaction state did not depend on individual reaction steps.

Discussion

The equilibrium constant of the TS reaction determined in this study, as well as those of the other reaction steps, that is, ATP binding,

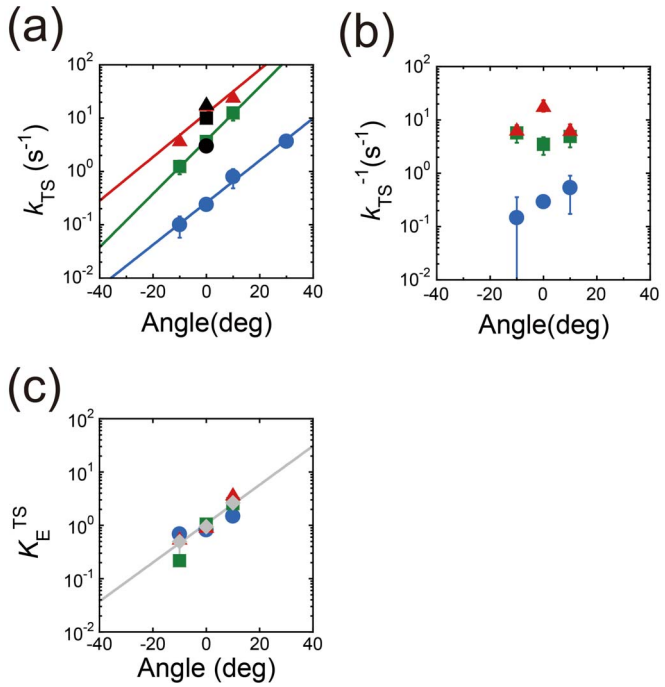

Figure 5 | Angular dependence of kinetic parameters. Angular dependence of k_{TS}^{on}, k_{TS}^{off}, and K_E^{TS} Blue circle, green square, and red triangle symbols represent the values for 18, 23, and 28°C, as determined from Figs. 4a, 4c, and 4e, respectively. In (a), the black symbols represent k_{TS}^{on} obtained from the freely rotating F_1s (Fig 2c). In (c), the gray symbols represent the average of K_E^{TS} for 18, 23, and 28°C.

hydrolysis, and P_i release, determined in our previous studies[15,31], are shown in Fig. 7. Data points are plotted in the angular diagram of the reaction scheme for one β subunit (Fig. 1), where the pause angles for ATP binding, TS reaction, hydrolysis, and P_i release were assigned as 0°, 0°, 200° and 320°, respectively. The magnitude of rotational torque (N) is determined by the slope of the rotational energy potential in the post-reaction state, $dU_{post}(\theta)/d\theta$[31,32]. It is very difficult to measure the rotational potential directly in the post-reaction state, $U_{post}(\theta)$. Therefore, in our previous studies, we had estimated the torque generated during each reaction step from the angular dependence of the reverse reaction rate, $\Delta G_1(\theta) = -k_BT\cdot[\ln k^{-1}(\theta)]$[31,32], which is a measure of the energy difference between the transition state and the post-reaction state, $\Delta G_1(\theta) = U_{post}(\theta) - U_{TS}(\theta)$. When we assume that the energy level at the transition state, $U_{TS}(\theta)$, is a constant, and does not depend on the rotational angle, the derivative of the energy difference responds to the slope of the potential in the post-reaction state (equivalent to the torque), $d\Delta G_1(\theta)/d\theta = dU_{post}(\theta)/d\theta$. Therefore, we previously estimated the torque generation from the reverse reaction rate based on this assumption with respect to the energy level for the transition state[31,32], which has not been verified experimentally so far. In this study, we used the angle dependence of the equilibrium constant, $K_E(\theta)$, which is a more robust approach to estimate the torque generation. The free energy difference between the pre- and post-reaction states can be determined from the angle dependence of the equilibrium constant; $\Delta G_2(\theta) = U_{post}(\theta) - U_{pre}(\theta) = k_BT\cdot[\ln(K_E(\theta))]$. Because $U_{pre}(\theta)$ was not affected by the elastic component located on the transmission line to the beads[9], and was almost the same for each reaction step (Fig. 6), the derivative of the free energy difference may be regarded as a measure of the slope of the rotational potential in the post-reaction state (equivalent to the torque), $d\Delta G_2(\theta)/d\theta \approx dU_{post}(\theta)/d\theta$. Therefore, the slopes of the equilibrium constants in a semi-log plot (Fig. 7) reflect the magnitude of torque generated upon each reaction step. The estimation shows that

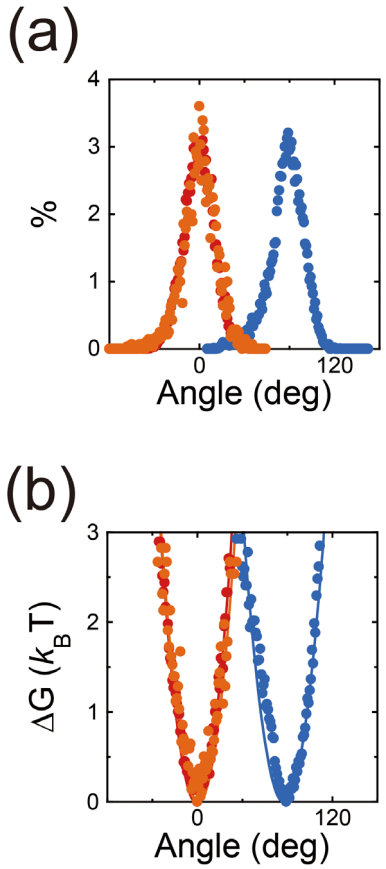

Figure 6 | Rotational energy potential. (a). Probability distributions of angular positions during the dwell. Red and blue points represent our previous results for the ATP binding dwell of wild-type F_1 and the hydrolysis dwell of mutant F_1, $\alpha_3\beta(E190D)_3\gamma$[31]. Orange points represent the experimental result for the TS dwell of mutant F_1 measured in this study. The probability distribution was derived from three molecules. (b). Rotational energy potentials determined from probability distribution according to the Boltzman's law, $\Delta G = -k_BT\cdot\ln(P/P_o)$. The potentials determined were fitted to the harmonic function $\Delta G = 1/2\cdot\kappa\cdot\theta^2$, where κ is the torsion stiffness. Stiffness values determined were 80, 75, and 64 pN·nm for the ATP binding of wild-type F_1, the TS reaction, and the hydrolysis of mutant F_1, respectively.

the TS reaction has a slope similar to those of ATP binding and P_i release and a steeper slope than that of ATP hydrolysis. This suggests that the contribution of the TS reaction to torque generation is similar to those of ATP binding and P_i release and is much higher than that of ATP hydrolysis, i.e., the TS reaction contributes significantly to the torque generation of F_1.

Considering the extremely high temperature dependence of the TS reaction, this reaction may involve a large-scale conformational rearrangement of the catalytic β-subunit when the γ is oriented to the angle for ATP binding. Recent single-molecule studies have revealed that the *C*-terminal region of the β subunit shows a large-scale conformational change at around 0°[5,33], which contributes to generating half of the rotational torque, that is, approximately 20 pN·nm rad^{-1}[34,35]. Our experimental results suggest that the TS reaction contributes greatly to torque generation at around 0°. Therefore, it is probable that the TS reaction is somehow related to the large-conformational change in the *C*-terminal region of the β subunit at 0°; however, there has been no direct verification so far. To identify the TS reaction, we hope to visualize simultaneously the conformational change in the β subunit and the rotational motion at the temperature, where F_1 shows a distinctive pause due to the TS reaction.

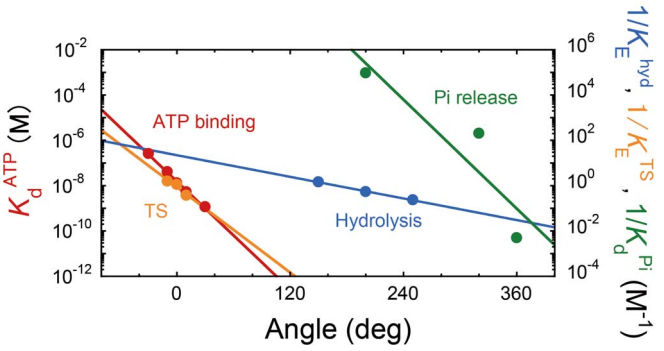

Figure 7 | Modulation of equilibrium constants upon γ rotation. Modulation of equilibrium constants upon rotation. All data points are plotted along the reaction scheme for one β subunit (Fig. 1), where the angles for ATP binding, TS reaction, hydrolysis, and P_i release are assigned as 0°, 0°, 200°, and 320°, respectively. Red, blue, and green symbols represent the dissociation constant of ATP (K_d^{ATP}), the inverse values of the equilibrium constant of ATP hydrolysis ($1/K_E^{Hyd}$), and the dissociation constant of P_i ($1/K_d^{Pi}$), determined in the previous study[15,22,31]. Orange symbols represent the inverse values of the equilibrium constant of the TS reaction ($1/K_E^{TS}$), determined in this study.

Improper ATP hydrolysis due to an alternative catalytic pathway[27] may be another possible reason for the occurrence of the TS reaction. According to this mechanism, P_i release in the β-subunit at the 320° state (cyan circle at 320° in Fig. 1) may drive the rotation of the 40° substep from 320° to 360° (=0°) without hydrolyzing ATP in another β-subunit at the 200° state (left green circle at 320° in Fig. 1). This may cause the dwell at 0° for waiting the ATP hydrolysis to occur in the aforementioned β-subunit at the 240° state (left green circle at 0° in Fig. 1). In our experimental data, the angle dependence of the rate constants of the TS reaction and its reverse reaction (Fig. 5) was similar to those of ATP hydrolysis and synthesis[31]. The forward reaction rate was accelerated towards the anticlockwise direction, while the reverse reaction rate was almost constant and did not depend on the rotary angle, although the slopes of angle dependence are different from each other. Therefore, our result suggests that the TS reaction might occur due to improper ATP hydrolysis at the 240° state (left green circle at 0° in Fig. 1). Simultaneous monitoring of the catalytic events, i.e., ATP binding, hydrolysis, and products release, with the rotational motion will provide insights into this mechanism.

Using single-molecule manipulations, we measured the rate and equilibrium constants of F_1 in the transient conformational states, which could not be obtained in the conventional single molecule assay. Moreover, from the equilibrium constants determined by single-molecule manipulations, we evaluated the force generated during the elementary reaction steps. Thus, single-molecule manipulation is a powerful tool for understanding the chemomechanical energy coupling mechanism and holds promise for understanding the functioning of other molecular machines.

Methods

Rotation assay. The mutant form of F_1 from thermophilic *Bacillus* PS3 (TF_1), $\alpha_3\beta(E190D)_3\gamma$, was prepared as described previously[36]. To visualize the rotation of F_1, the stator region ($\alpha_3\beta_3$ subunits) was fixed to a glass surface, and magnetic beads (ϕ approximately 0.3 μm; Seradyn, USA) were attached to the rotor (γ subunit), as the probe for monitoring rotation and for further manipulation. The rotation assay was carried out in a 50 mM MOPS-KOH (pH 7.0) buffer containing 50 mM KCl, 5 mM $MgCl_2$, and 1 mM ATP. Rotating beads were observed under a phase-contrast microscope (IX-70 or IX-71; Olympus, Japan) with a 100× objective lens. The temperature in the room was controlled with a room air conditioner and monitored with a thermometer located on the sample stage of the microscope. The precision of the temperature control was ±1°C.

Manipulation with magnetic tweezers. The stage of the microscope was equipped with magnetic tweezers that could be controlled with the custom-made software

(Celery, Library, Japan). The rotation of the bead was simultaneously recorded at 30 and 1,000–3,000 frames/s (FC300M, Takex; FASTCAM 1024PCI-SE, Photoron, Japan). Images were stored in the HDD of a computer as AVI files and analyzed using the custom-made software.

1. Yoshida, M., Muneyuki, E. & Hisabori, T. ATP synthase - a marvellous rotary engine of the cell. *Nat Rev Mol Cell Biol* **2**, 669–77 (2001).
2. Junge, W., Sielaff, H. & Engelbrecht, S. Torque generation and elastic power transmission in the rotary F_oF_1-ATPase. *Nature* **459**, 364–70 (2009).
3. Weber, J. Structural biology: Toward the ATP synthase mechanism. *Nat Chem Biol* **6**, 794–5 (2010).
4. Dimroth, P., von Ballmoos, C. & Meier, T. Catalytic and mechanical cycles in F-ATP synthases. Fourth in the Cycles Review Series. *EMBO Rep* **7**, 276–82 (2006).
5. Abrahams, J. P., Leslie, A. G., Lutter, R. & Walker, J. E. Structure at 2.8 Å resolution of F_1-ATPase from bovine heart mitochondria. *Nature* **370**, 621–8 (1994).
6. Cingolani, G. & Duncan, T. M. Structure of the ATP synthase catalytic complex (F_1) from Escherichia coli in an autoinhibited conformation. *Nat Struct Mol Biol* **18**, 701–7 (2011).
7. Kabaleeswaran, V., Puri, N., Walker, J. E., Leslie, A. G. & Mueller, D. M. Novel features of the rotary catalytic mechanism revealed in the structure of yeast F_1 ATPase. *EMBO J* **25**, 5433–42 (2006).
8. Noji, H., Yasuda, R., Yoshida, M. & Kinosita, K., Jr. Direct observation of the rotation of F_1-ATPase. *Nature* **386**, 299–302 (1997).
9. Sielaff, H. *et al.* Domain compliance and elastic power transmission in rotary F_oF_1-ATPase. *Proc Natl Acad Sci U S A* **105**, 17760–5 (2008).
10. Spetzler, D. *et al.* Single molecule measurements of F_1-ATPase reveal an interdependence between the power stroke and the dwell duration. *Biochemistry* **48**, 7979–85 (2009).
11. Yasuda, R., Noji, H., Kinosita, K., Jr. & Yoshida, M. F_1-ATPase is a highly efficient molecular motor that rotates with discrete 120 degree steps. *Cell* **93**, 1117–24 (1998).
12. Cherepanov, D. A. & Junge, W. Viscoelastic dynamics of actin filaments coupled to rotary F-ATPase: curvature as an indicator of the torque. *Biophys J* **81**, 1234–44 (2001).
13. Bilyard, T. *et al.* High-resolution single-molecule characterization of the enzymatic states in Escherichia coli F_1-ATPase. *Philos Trans R Soc Lond B Biol Sci* **368**, 20120023 (2013).
14. Toyabe, S. *et al.* Nonequilibrium Energetics of a Single F_1-ATPase Molecule. *Phys Rev Lett* **104** (2010).
15. Watanabe, R., Iino, R. & Noji, H. Phosphate release in F_1-ATPase catalytic cycle follows ADP release. *Nat Chem Biol* **6**, 814–820 (2010).
16. Shimo-Kon, R. *et al.* Chemo-mechanical coupling in F_1-ATPase revealed by catalytic site occupancy during catalysis. *Biophys J* **98**, 1227–36 (2010).
17. Rees, D. M., Montgomery, M. G., Leslie, A. G. & Walker, J. E. Structural evidence of a new catalytic intermediate in the pathway of ATP hydrolysis by F_1-ATPase from bovine heart mitochondria. *Proc Natl Acad Sci U S A* **109**, 11139–43 (2012).
18. Ariga, T., Muneyuki, E. & Yoshida, M. F_1-ATPase rotates by an asymmetric, sequential mechanism using all three catalytic subunits. *Nat Struct Mol Biol* **14**, 841–6 (2007).
19. Yasuda, R., Noji, H., Yoshida, M., Kinosita, K., Jr. & Itoh, H. Resolution of distinct rotational substeps by submillisecond kinetic analysis of F_1-ATPase. *Nature* **410**, 898–904 (2001).
20. Shimabukuro, K. *et al.* Catalysis and rotation of F_1 motor: cleavage of ATP at the catalytic site occurs in 1 ms before 40 degree substep rotation. *Proc Natl Acad Sci U S A* **100**, 14731–6 (2003).
21. Nishizaka, T. *et al.* Chemomechanical coupling in F_1-ATPase revealed by simultaneous observation of nucleotide kinetics and rotation. *Nat Struct Mol Biol* **11**, 142–8 (2004).
22. Adachi, K. *et al.* Coupling of rotation and catalysis in F_1-ATPase revealed by single-molecule imaging and manipulation. *Cell* **130**, 309–21 (2007).
23. Martin, J. L., Ishmukhametov, R., Hornung, T., Ahmad, Z. & Frasch, W. D. Anatomy of F_1-ATPase powered rotation. *Proc Natl Acad Sci U S A* **111**, 3715–20 (2014).
24. Adachi, K., Oiwa, K., Yoshida, M., Nishizaka, T. & Kinosita, K. Controlled rotation of the F_1-ATPase reveals differential and continuous binding changes for ATP synthesis. *Nat Commun* **3** (2012).
25. Watanabe, R., Iino, R., Shimabukuro, K., Yoshida, M. & Noji, H. Temperature-sensitive reaction intermediate of F_1-ATPase. *EMBO Rep* **9**, 84–90 (2008).
26. Enoki, S., Watanabe, R., Iino, R. & Noji, H. Single-molecule Study on the Temperature-sensitive Reaction of F_1-ATPase with a Hybrid F_1 Carrying a Single β (E190D). *J Biol Chem* **284**, 23169–76 (2009).
27. Shimabukuro, K., Muneyuki, E. & Yoshida, M. An alternative reaction pathway of F_1-ATPase suggested by rotation without 80 degrees/40 degrees substeps of a sluggish mutant at low ATP. *Biophys J* **90**, 1028–1032 (2006).
28. Ohtsubo, M. *et al.* In vitro mutated beta subunits from the F_1-ATPase of the thermophilic bacterium, PS3, containing glutamine in place of glutamic acid in positions 190 or 201 assembles with the alpha and gamma subunits to produce inactive complexes. *Biochem Biophys Res Commun* **146**, 705–10 (1987).
29. Park, M. Y., Omote, H., Maeda, M. & Futai, M. Conserved Glu-181 and Arg-182 residues of Escherichia coli H^+-ATPase (ATP synthase) beta subunit are essential for catalysis: properties of 33 mutants between beta Glu-161 and beta Lys-201 residues. *J Biochem* **116**, 1139–45 (1994).
30. Senior, A. E. & al-Shawi, M. K. Further examination of seventeen mutations in Escherichia coli F_1-ATPase beta-subunit. *J Biol Chem* **267**, 21471–8 (1992).
31. Watanabe, R. *et al.* Mechanical modulation of catalytic power on F_1-ATPase. *Nat Chem Biol* **8**, 86–92 (2012).
32. Watanabe, R. & Noji, H. Chemomechanical coupling mechanism of F_1-ATPase: catalysis and torque generation. *FEBS Lett* **587**, 1030–5 (2013).
33. Masaike, T., Koyama-Horibe, F., Oiwa, K., Yoshida, M. & Nishizaka, T. Cooperative three-step motions in catalytic subunits of F_1-ATPase correlate with 80 degrees and 40 degrees substep rotations. *Nat Struct Mol Biol* **15**, 1326–33 (2008).
34. Tanigawara, M. *et al.* Role of the DELSEED Loop in Torque Transmission of F_1-ATPase. *Biophys J* **103**, 970–8 (2012).
35. Usukura, E. *et al.* Torque Generation and Utilization in Motor Enzyme F_oF_1-ATP Synthase Half-torque F_1 with short-sized pushrod helix and reduced ATP synthesis by half-torque F_oF_1. *J Biol Chem* **287**, 1884–1891 (2012).
36. Okuno, D., Iino, R. & Noji, H. Stiffness of gamma subunit of F_1-ATPase. *Eur Biophys J* **39**, 1589–96 (2010).

Acknowledgments

We thank all members of the Noji Laboratory. This work was supported by Grant-in-Aid for Scientific Research no. 18074005 to H.N. and no. 30540108 to R.W. from the Ministry of Education, Culture, Sports, Science, and Technology, Japan, and Precursory Research for Embryonic Science to R.W. from the Japan Science and Technology Agency.

Author contributions

R. W. designed and performed the experiments and analyzed the data; H. N. designed the experiments, built the whole story, and wrote the paper with R.W.

Additional information

Competing financial interests: The authors declare no competing financial interests.

How to cite this article: Watanabe, R. & Noji, H. Characterization of the temperature-sensitive reaction of F_1-ATPase by using single-molecule manipulation. *Sci. Rep.* **4**, 4962; DOI:10.1038/srep04962 (2014).

This work is licensed under a Creative Commons Attribution 3.0 Unported License. The images in this article are included in the article's Creative Commons license, unless indicated otherwise in the image credit; if the image is not included under the Creative Commons license, users will need to obtain permission from the license holder in order to reproduce the image. To view a copy of this license, visit http://creativecommons.org/licenses/by/3.0/